UAV Mapping for Multiple Primary Users Localization

Zhuyin Li*, Andrea Giorgetti†, and Sithamparanathan Kandeepan*

*School of Engineering, RMIT University, Melbourne, Australia
†DEI, University of Bologna, Italy
Email: s3666118@student.rmit.edu.au, {a.giorgetti, kandeepan}@ieee.org

***Abstract*—The unique features of unmanned aerial vehicles (UAVs) extend a large number of existing technologies into environments that are not suitable for on-site operations. Localization, a critical basis of many applications such as cognitive radio and first response networks, can benefit UAV technology as well. In such scenarios, an underinvestigated problem is the non-collaborative localization of multiple primary users (PUs). Therefore, this work proposes a data-driven multiple PU localization algorithm based on the angular and power measurements performed by a UAV equipped with an antenna array. The measured data firstly generate a score map, then a threshold and a hierarchical clustering method are applied to the score map to both detect the number of PUs and estimate their location. The performance of the algorithm is assessed by numerical results in terms of probability of detecting the number of PUs, and root-mean-square-error of position estimation. The proposed solution exhibit remarkable performance considering that the approach requires only the knowledge of the PUs frequency band.**

I. Introduction

Unmanned aerial vehicles (UAVs) have been regarded as a significant extension of the existing terrestrial wireless communication networks. UAV-aided wireless communication possesses unique features, e.g., high mobility, fast deployment, flexible configuration, with the presence of short-range line-of-sight (LoS) path, enabling many more possibilities for the design and implementation of networks [1]. Similarly, compared with traditional techniques, UAV-aided localization techniques can minimize the challenge from geographical conditions, network deployment, hazard risks, etc.

On the other hand, among the many localization types, the position estimation of non-collaborative multiple primary users (PUs) is one of the most arduous. The conventional localization techniques based on time of arrival (ToA) or time difference of arrival (TDoA) cannot be utilized in this situation [2], [3]. Some of the well developed non-collaborative localization techniques normally depend on the pre-built fingerprinting database [4], received signal strength (RSS) [5]–[7], and direction of arrival (DoA) [8]. Although these methods work well for single PU localization, they can hardly be extended to multiple PUs scenarios due to their simultaneous transmission. A known solution to this problem is to find the maximum likelihood estimates of the PU locations [9]–[11]. Unfortunately, apart from the high computational complexity for the expectation-maximization (EM) iterations, such an approach requires knowledge of the number of PUs. An alternative approach is presented in [12], where two UAV-assisted methods to localize multiple radiation sources are proposed. However, it remains unexplored if the technique can be applied to the radio-frequency (RF) scenarios.

To tackle the existing gap in the UAV-aided multiple PU localization research, we propose a data-driven localization technique. In particular, our main contributions can be summarized as follows:

- We propose a localization algorithm based on the RSS and sector of arrival (SoA) measurements from multiple PUs.
- Based on the RSS and SoA collected by the UAV, the algorithm builds a score map from which simultaneously estimates the number of PUs as well as their positions.
- The performance of the localization algorithm is evaluated by Monte-Carlo simulations in terms of the probability of detecting PUs and the root-mean-square error (RMSE) of position estimation.

The remainder of the paper is organized as follows. In Section II, the general system model of the problem is presented. The proposed algorithm is discussed in Section III. The specific case study is illustrated in Section IV, followed by the performance evaluation in Section V. Conclusions are drawn in Section VI.

II. System Model

In this paper, we consider the non-collaborative localization of simultaneously transmitting PUs employing a single UAV. Without loss of generality, let us consider N PUs at unknown positions, $\mathbf{l}_{\mathrm{p}}^{j} = [x_{\mathrm{p}}^{j}, y_{\mathrm{p}}^{j}]^{T}$, $j = 1, ..., N$, within a square area of side length $\mathscr{L}$, as shown in Fig. 1. PUs are static and have identical transmit power and carrier frequency. The UAV cruises over the area, listening to the signals transmitted by the PUs and taking M measurements along its pre-planned trajectory to perform localization. The UAV is equipped with a positioning system, an RSS sensor, and a uniform linear array (ULA). Therefore, each measurement data set, $\mathcal{M}^{i}$, includes four pieces of information, $\mathcal{M}^{i} = \{\mathbf{l}^{i}, \eta^{i}, \mathbf{s}^{i}, \mathbf{p}^{i}\}$, $i = 1, ..., M$, where $\mathbf{l}^{i} = [x^{i}, y^{i}]^{T}$ and η^{i} are the UAV location and heading direction angle respectively, while $\mathbf{s}^{i}$ and $\mathbf{p}^{i}$ are vectors, keeping track of the SoAs and their corresponding RSSs. The definition and construction of these two vectors will be given later in this section.

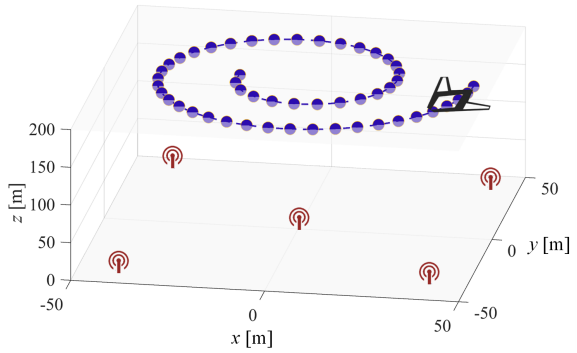

Fig. 1. System model: the UAV is flying along the blue trajectory. The points are locations where the measurements are performed, and the five red transmitters are the ground-based PUs to be located.

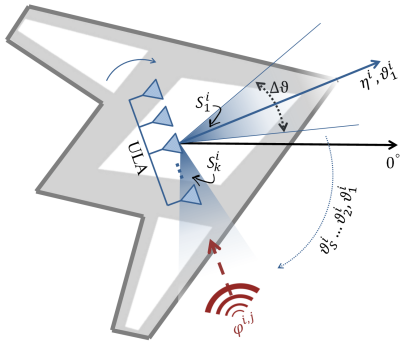

Fig. 2. The ULA on the UAV and the polar coordinate system. The blue parts are the ULA beam and sectors and the red parts represent an example of the incident signal from one of the PUs.

Fig. 2 illustrates the ULA antenna model and the ground-based coordinate system with the global 0°. The ULA is electronically steered step-by-step with a step size equal to the beamwidth, $\Delta\vartheta$, to cover 2π. As a result, the rotation generates $S = \frac{2\pi}{\Delta\vartheta}$ sectors, with the boresight direction of the kth sector $\vartheta_k = \vartheta_1 + \Delta\vartheta(k-1)$, $k = 1, \ldots, S$. For each measurement, the boresight direction of the first sector is always aligned with the heading direction of the UAV, i.e., $\vartheta_1^i = \eta^i$. By neglecting secondary effects due to specific antenna patterns, the receiver antenna gain can be approximated as [13]

$$\mathrm{G_R}(\varphi^{i,j}, \mathcal{S}_k^i) = \begin{cases} \mathrm{G_R}, & \varphi^{i,j} \in \mathcal{S}_k^i \\ 0, & \text{otherwise} \end{cases} \tag{1}$$

where $\mathcal{S}_k^i = [\vartheta_k^i - \frac{\Delta\vartheta}{2}, \vartheta_k^i + \frac{\Delta\vartheta}{2}]$, and

$$\varphi^{i,j} = \arctan\left(\frac{y_\mathrm{p}^j - y^i}{x_\mathrm{p}^j - x^i}\right) \tag{2}$$

is the DoA.[1] Since the proposed algorithm only requires the received sector indexes, r, instead of the precise DoA, the measurement consists of a SoA vector collecting the sector indexes corresponding to $\varphi^{i,j}$. More specifically, we denote the SoA vector as $\mathbf{s}^i = [s_1^i, \ldots, s_R^i]^\mathrm{T}$, in which $s_r^i = k$, if $\varphi^{i,j} \in \mathcal{S}_k^i$, where R is the actual number of sectors receiving power from PUs. Note that due to the unknown locations of the sources, in some cases the DoA can be within the same sector, so that $R \leq \min\{N, S\}$. Accordingly, the vector of received power is $\mathbf{p}^i = [P_1^i, P_2^i, \ldots, P_R^i]^\mathrm{T}$, where P_r^i is the RSS at sector r and measurement i. We denote with $P_r^{i,j}$ the RSS from the jth PU measured at sector r and location $\mathbf{l}^i$ as

$$P_r^{i,j}(\varphi^{i,j}) = \frac{P_\mathrm{T}\mathrm{G_T}\mathrm{G_R}(\varphi^{i,j}, \mathcal{S}_r^i)}{\mathrm{PL}(||\mathbf{l}_\mathrm{p}^j - \mathbf{l}^i||_2)} \tag{3}$$

where P_T is the PU transmit power, $\mathrm{G_T}$ is the transmit antenna gain considered isotropic, and $\mathrm{PL}(d)$ is the path-loss at distance d. In the presence of N PUs, the RSS within the rth sector is

$$P_r^i = \sum_{j=1}^{N} P_r^{i,j}\, \mathbb{1}\{\varphi^{i,j} \in \mathcal{S}_r^i\} \tag{4}$$

where $\mathbb{1}\{\cdot\}$ is the indicator function, i.e., its value is 1 when the argument is true and 0 otherwise. In this work, our algorithm is not constrained to any specific channel model, so the PL can be represented by any propagation law that is suitable for the environment, e.g., the power-law path-loss with log-normal shadowing, the directional channel model [14], and the air-to-ground channel model [15], [16].

III. UAV Mapping, Detection and Localization

Let us divide the square area into $g \times g$ grid points with spacing $\Delta_\mathrm{g} = \mathscr{L}/(g-1)$. The UAV takes the M measurements along its pre-planned trajectory with a step of length Δ_m. The proposed UAV-aided multiple PU localization technique can be divided into two phases: 1) score map construction; 2) hierarchical clustering and weighted centroid (HCWC) technique for detection and localization of the PUs.

A. Score Map Construction

We construct a score map, based on the SoA and RSS, whose peaks represent the PU number and positions. Details are shown from line 1 to line 15 in Algorithm 1. Here is the summary of the main steps to build the score map:

1) Measurements collection, $\mathcal{M}^i = \{\mathbf{l}^i, \eta^i, \mathbf{s}^i, \mathbf{p}^i\}$.
2) Calculate the boresight direction per sector for each measurement, $\vartheta_k^i = \eta^i + (k-1)\Delta\vartheta$.
3) Dividing the area equally into $g \times g$ grid points with coordinates $\mathbf{l}_{m,n} = [x_m, y_n]^T$, the angle seen from the ith measurement position to the grid point is $\varphi_{m,n}^i = \arctan\left(\frac{y_n - y^i}{x_m - x^i}\right)$.
4) Assign the RSS, (4), as the score value to the grid points falling within the SoA and zero to the rest. Thus the score value at the grid point $\mathbf{l}_{m,n}$ at measurement i is given by

$$\mathfrak{S}_{m,n}^i = \begin{cases} P_r^i, & \vartheta_{s_r^i}^i - \frac{\Delta\vartheta}{2} \leq \varphi_{m,n}^i \leq \vartheta_{s_r^i}^i + \frac{\Delta\vartheta}{2} \\ 0, & \text{otherwise.} \end{cases} \tag{5}$$

[1] We denote with $\arctan(\cdot)$ the four-quadrant inverse tangent.

5) Sum up the score as per measurement at each grid point, $\mathfrak{S}_{m,n} = \sum_{i=1}^{M} \mathfrak{S}_{m,n}^{i}$.

B. Hierarchical Clustering and Weighted Centroid Method

To analyze the score map, we propose the HCWC technique to estimate the number and positions of PUs with no extra prerequisites. Two pre-defined parameters, the threshold α (dimensionless) and the cutoff distance D_{cut} (in meters) are needed for the algorithm. Their values should be determined by the specific environment, e.g., the size of the area, the RSS level of the score map, etc. HCWC is shown from line 16 to line 29 in Algorithm 1, and here summarized:

6) Calculate the threshold for the score map, $\mathfrak{S}_{\text{th}} = \alpha \mathfrak{S}_{\text{max}}$, where $\mathfrak{S}_{\text{max}} = \max_{m,n}\{\mathfrak{S}_{m,n}\}$.
7) Generate a new sub-map $\bar{\mathfrak{S}}_{m,n}$ by removing the grid points with score values below the threshold $\mathfrak{S}_{\text{th}}$.
8) Group the grid points in the map $\bar{\mathfrak{S}}_{m,n}$ by hierarchical clustering, given the cut off distance, D_{cut}, as the shortest distance between clusters. The cluster number per grid point is denoted as $\mathfrak{C}_{m,n}$.
9) The estimation of the number of PUs is given by the number of surviving clusters, $\hat{N} = \max_{m,n}\{\mathfrak{C}_{m,n}\}$.
10) The PU positions are estimated by weighted centroid localization (WCL) among all the grid points within the cluster [5]. We denote the position of the grid points in the $\mathfrak{C}_{m,n}$ cluster as $\mathbf{l}_{m_c,n_c} = [x_{m_c}, y_{n_c}]$, with $m_c, n_c = 1, \ldots, N_c$, where N_c the number of grid points within the cluster and $c = 1, \ldots, \hat{N}$. Therefore, the estimation of the PU position from the cth cluster is given by [17]

$$\hat{\mathbf{l}}_{\text{p}}^{c} = [\hat{x}_{\text{p}}^{c}, \hat{y}_{\text{p}}^{c}] = \left[\frac{\sum_{m_c=1}^{N_c} \omega_{m_c} x_{m_c}}{\sum_{m_c=1}^{N_c} \omega_{m_c}}, \frac{\sum_{n_c=1}^{N_c} \omega_{n_c} y_{n_c}}{\sum_{n_c=1}^{N_c} \omega_{n_c}} \right] \tag{6}$$

where the weighting coefficient is

$$\omega_{m_c,n_c} = \frac{\mathfrak{S}_{m_c,n_c} - \mathfrak{S}_{\text{min}}}{\mathfrak{S}_{\text{max}} - \mathfrak{S}_{\text{min}}} \tag{7}$$

with $\mathfrak{S}_{\text{min}} = \min_{m,n}\{\mathfrak{S}_{m,n}\}$.

Algorithm 1 Mapping, Detection and Localization

1: Get $\mathcal{M}^i = \{\mathbf{l}^i, \eta^i, \mathbf{s}^i, \mathbf{p}^i\}$, $i = 1, \ldots, M$
2: **for all** $\mathcal{M}^i$ such that $i = 1 : M$ **do**
3: $\quad \vartheta_k^i \leftarrow \eta^i + (k-1)\Delta\vartheta, k = 1, ..., S$
4: $\quad$ **for all** $\mathbf{l}_{m,n}$ such that $m = 1, ..., g, n = 1, ..., g$ **do**
5: $\quad\quad \varphi_{m,n}^i \leftarrow \arctan\left(\frac{y_n - y^i}{x_m - x^i}\right)$
6: $\quad\quad$ **for all** r such that $r = 1, ..., R$ **do**
7: $\quad\quad\quad$ **if** $\varphi_{m,n}^i \in [\vartheta_{S_r^i}^i - \frac{\Delta\vartheta}{2}, \vartheta_{S_r^i}^i + \frac{\Delta\vartheta}{2}]$ **then**
8: $\quad\quad\quad\quad \mathfrak{S}_{m,n}^i \leftarrow P_r^i$
9: $\quad\quad\quad$ **else**
10: $\quad\quad\quad\quad \mathfrak{S}_{m,n}^i \leftarrow 0$
11: $\quad\quad\quad$ **end if**
12: $\quad\quad$ **end for**
13: $\quad$ **end for**
14: $\quad \mathfrak{S}_{m,n} \leftarrow \sum_{i=1}^{M} \mathfrak{S}_{m,n}^i$
15: **end for**
16: $\mathfrak{S}_{\text{max}} \leftarrow \max_{m,n}\{\mathfrak{S}_{m,n}\}$
17: $\mathfrak{S}_{\text{th}} \leftarrow \alpha \mathfrak{S}_{\text{max}}$
18: **for all** $\mathfrak{S}_{m,n}$ **do**
19: $\quad$ **if** $\mathfrak{S}_{m,n} \geq \mathfrak{S}_{\text{th}}$ **then**
20: $\quad\quad \bar{\mathfrak{S}}_{m,n} \leftarrow \mathfrak{S}_{m,n}$
21: $\quad$ **else**
22: $\quad\quad \bar{\mathfrak{S}}_{m,n} \leftarrow$ null
23: $\quad$ **end if**
24: **end for**
25: $\mathfrak{C}_{m,n} \leftarrow \text{Cluster}\{\bar{\mathfrak{S}}_{m,n} | D_{\text{cut}}\}$
26: $\hat{N} \leftarrow \max_{m,n}\{\mathfrak{C}_{m,n}\}$
27: **for all** $\mathfrak{C}_{m,n} = 1, ..., \hat{N}$ **do**
28: $\quad \hat{\mathbf{l}}_{\text{p}}^{c} = [\hat{x}_{\text{p}}^{c}, \hat{y}_{\text{p}}^{c}] = \left[\frac{\sum_{m_c=1}^{N_c} \omega_{m_c} x_{m_c}}{\sum_{m_c=1}^{N_c} \omega_{m_c}}, \frac{\sum_{n_c=1}^{N_c} \omega_{n_c} y_{n_c}}{\sum_{n_c=1}^{N_c} \omega_{n_c}} \right]$
29: **end for**

IV. Case Study

In this section, we introduce the simulation settings, including the channel model, the UAV trajectory, and the parameters used in the algorithms.

A. Channel model

We adopt the A2G channel model proposed for an airborne scenario [15]. The path-loss under the A2G channel can be defined as the summation of excessive path-loss component and the free space path-loss, $\text{PL}(d) = \varepsilon + \text{FSPL}(d)$, when expressed in decibel. The free space path-loss can be calculated by Friis transmission equation. The term, ε, follows a normal distribution with mean, μ_ξ, and standard deviation, $\sigma_\xi(\lambda)$, where ξ is the group number, 1 for LoS, or 2 for none-line-of-sight (NLoS). The mean, μ_ξ, is a constant, independent from the elevation angle. The standard deviation can be described by $\sigma_\xi(\lambda) = a_\xi \exp(-b_\xi \lambda)$, where a_ξ and b_ξ are frequency and environment-dependent parameters, while λ is the elevation angle in degrees. The occurrence probability of each group can be defined as $p_\lambda(1) = c \cdot (\lambda - \lambda_0)^d$ and $p_\lambda(2) = 1 - p_\lambda(1)$, where λ_0 is selected as 15° corresponding to the minimum elevation angle supported by the model. In our case, we adopt the parameter values recommended for the urban scenario at $f = 2\,\text{GHz}$: $\mu_1 = 1.0$, $\mu_2 = 20$, $a_1 = 10.39$, $b_1 = 0.05$, $a_2 = 29.6$, $b_2 = 0.03$, $c = 0.6$, and $d = 0.11$. Parameters for other scenarios can be found in Table II of [15].

B. UAV trajectory

The UAV flies over the area following an Archimedean spiral expressed by the equation, $\mathfrak{r} = \mathfrak{a} + \mathfrak{b}\theta$, in the polar coordinate system $(\mathfrak{r}, \theta)$, where $\mathfrak{a}$ and $\mathfrak{b}$ control the turns and the distance between each turn, respectively. Assuming the inner end of the spiral is fixed at $[x_0, y_0]$, $\mathfrak{a} = x_0$, and $\mathfrak{b} = \frac{\mathfrak{g}}{2\pi}$, where $\mathfrak{g}$ is the spiral growth per turn. The total length of the spiral is

$$\mathfrak{L} = \int_{\pi}^{2\mathfrak{t}\pi} \sqrt{(\mathfrak{a} + \mathfrak{b}\theta)^2 + \mathfrak{b}^2}\, d\theta \tag{8}$$

where $\mathfrak{t}$ is the number of turns of the spiral. Then, the spacing of the measurements along the spiral is $\Delta_{\text{m}} = \frac{\mathfrak{L}}{M} \approx \mathfrak{r}^i \sin\Delta_\theta^i$,

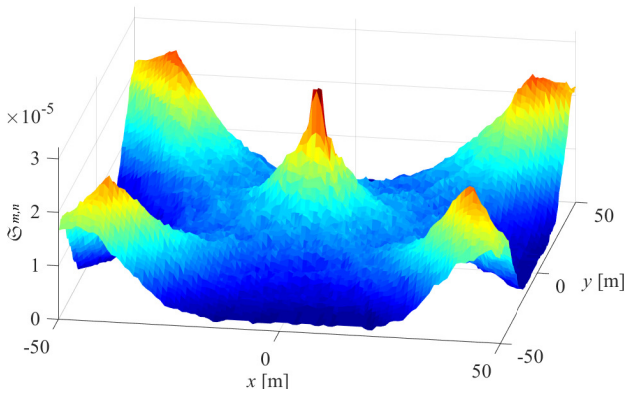

Fig. 3. An example of the score map $\mathfrak{S}_{m,n}$ for the five PUs scenario depicted in Fig. 1.

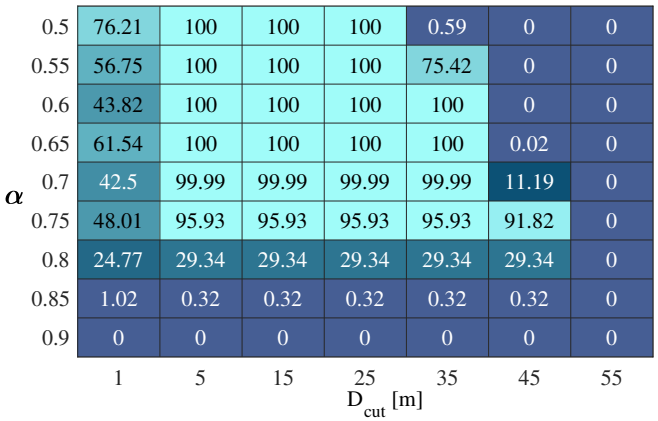

Fig. 4. The impact of α and D_{cut} in terms of probability of detecting the PUs, $\mathscr{P}_{\text{D}}^{N}$, in percentage.

where Δ_{m} can be regarded as the length increment of the spiral at each step, and Δ_θ is the angular increment. If we keep Δ_{m} constant, with the spiral growing bigger, Δ_θ for each step is getting smaller. Therefore, the iteration of the increment is, $\Delta_\theta^i \approx \Delta_\theta^{i-1} + \arcsin(\Delta_{\text{m}}^{i-1}/\mathfrak{r}^i)$. Note that such definition can only be true when Δ_θ is relatively a small angle, so that the arc length with respect to Δ_θ can be estimated as $\mathfrak{r}\sin\Delta_\theta$. Note that the heading direction of the UAV η^i is the tangent line to the spiral.

C. System overview

As shown in Fig. 1, we consider five PUs located exactly at $[42, 40; -39, 41; -40, -41; 41, -38; 0, 1]$ m within a square area of side length $\mathscr{L} = 100$ m and grid spacing $\Delta_{\text{g}} = 1$ m. The transmit power P_{T} of each PU is 0 dBW. The UAV trajectory is fixed with the ending point at $[5, 0]$ m, the number of turns is $\mathfrak{t} = 2$, and the spiral growth is $\mathfrak{g} = 20$ m, to cover the area with a reasonable trajectory length. The beamwidth of the ULA is $\Delta\vartheta = 15°$. All the results are obtained by Monte-Carlo simulations with $T = 10^6$ runs to account for different channel realizations. Following Algorithm 1, the score map of this scenario is created, and an example is shown in Fig. 3. Intuitively, the five peaks illustrated by the score map are due to the PUs. The HCWC algorithm is then applied to estimate the number of PUs and their locations.

V. Performance Evaluation

In this section, we evaluate the performance of the proposed localization algorithm in terms of two aspects: the probability of detecting u PUs, $\mathscr{P}_{\text{D}}^{u}$, and the RMSE of their position estimation, $\mathscr{E}_{\text{pos}}^{u}$. Given that the estimate of the PU number is $\hat{N}$, the above probability of detection is

$$\mathscr{P}_{\text{D}}^{u} = \mathbb{P}\{\hat{N} = u\} \simeq \frac{\mathbb{N}\{u\}}{T} \tag{9}$$

where $\mathbb{N}\{u\}$ is the number of Monte-Carlo realizations resulting in u. The corresponding RMSE is given by

$$\mathscr{E}_{\text{pos}}^{u} = \sqrt{\frac{1}{\mathbb{N}\{u\}\min\{N,u\}} \sum_{t=1}^{\mathbb{N}\{u\}} \sum_{c=1}^{\min\{N,u\}} \left\| \hat{\mathbf{l}}_{\text{p}}^{c} - \mathbf{l}_{\text{p}}^{c} \right\|_2^2} \tag{10}$$

where $\hat{\mathbf{l}}_{\text{p}}^{c}$ is the PU location estimate from the tth Monte-Carlo run. To simplify the scenarios and to display the data clearly, we consider only three cases, $\hat{N} = N-1$, $\hat{N} = N$, $\hat{N} = N+1$ with probabilities, $\mathscr{P}_{\text{D}}^{N-1}$, $\mathscr{P}_{\text{D}}^{N}$, $\mathscr{P}_{\text{D}}^{N+1}$, and localization error, $\mathscr{E}_{\text{pos}}^{N-1}$, $\mathscr{E}_{\text{pos}}^{N}$, $\mathscr{E}_{\text{pos}}^{N+1}$, respectively. For comparison, the scenario is decomposed into u single PU localization problems [13], and the RMSE, $\mathscr{E}_{\text{pos}}^{\text{sgl}}$, is given by averaging the RMSE of each single localization. The algorithm performance is investigated concerning three aspects, the impact of algorithm parameters, α, D_{cut}, and M, and UAV position uncertainty.

A. Impact of α and D_{cut}

According to Algorithm 1, α determines which grid points can be selected for successive clustering, and D_{cut} determines how these grid points are merged into each cluster. The impact of these two parameters is schematically shown in Fig. 4 with respect to the probability of detecting the PUs, $\mathscr{P}_{\text{D}}^{N}$, with $M = 100$ measurements. As expected, the increase in α leads to a decrease in $\mathscr{P}_{\text{D}}^{N}$, and the number of PUs is underestimated. The reason is that with the increase in the threshold, some grid points presenting one or more peaks in the score map are likely to be eliminated from the clustering process. Similarly, large D_{cut} forces cluster merging, which again leads to PUs number underestimation and a drop of $\mathscr{P}_{\text{D}}^{N}$. Therefore, in the following, we consider $\alpha = 0.6$ and $D_{\text{cut}} = 15$ m.

B. Impact of the number of measurements

In this section, we investigate how the number of measurements affects the performance of the algorithm. Keeping fixed the UAV starting point and step size $\Delta_{\text{m}} = 3.18$ m, the increase of M leads to a longer trajectory and better coverage of the area. Fig. 5 depicts the probability of estimating the PU number (bar chart on the right) and the RMSE (line chart on the left). For M less than 40, $\mathscr{P}_{\text{D}}^{N-1}$ is almost 100%, while with M exceeding 40, the correct PU number estimation can be guaranteed. The value of $\mathscr{P}_{\text{D}}^{N+1}$ can hardly be noticed for all the values of M. Regarding the localization error, the RMSE decreases when M increases from 20 to 40, then it exhibits a floor of about 1 m with a larger M. Remarkably,

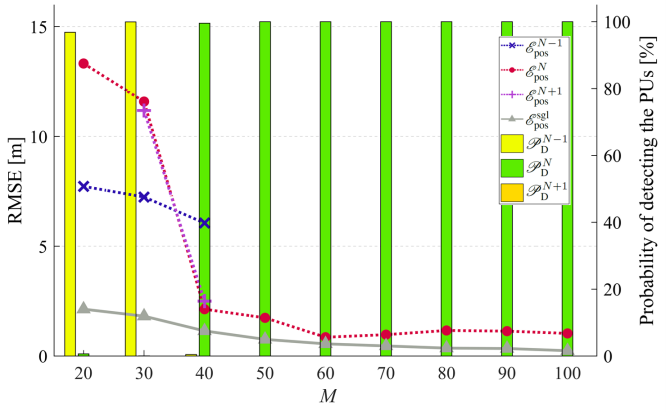

Fig. 5. The probability of detecting the PUs and the RMSE of localization error, with respect to the number of measurements M under three cases: $\hat{N} = N-1, \hat{N} = N, \hat{N} = N+1$.

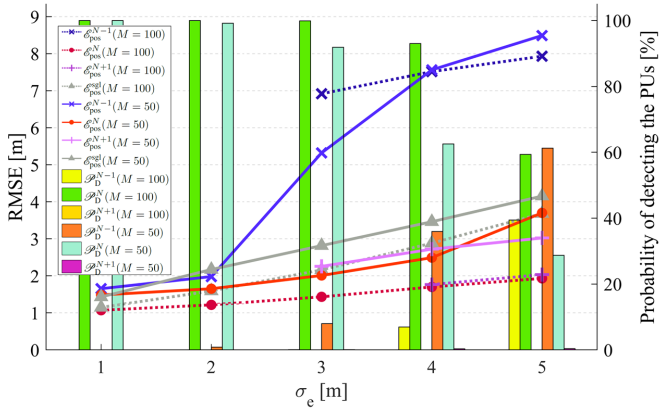

Fig. 6. The impact of the UAV position uncertainty on the RMSE and the probability of detecting the PUs.

the performance of the proposed solution with multiple PUs is only slightly worse, in terms of RMSE $\mathscr{E}_{\text{pos}}^{\text{sgl}}$, than the single PU localization.

C. Impact of UAV position uncertainty

The error vector, $\mathbf{e} = [e_x, e_y]^T$, led by the uncertainties of the positioning device (e.g., GPS), has independent components, e_x and e_y, following a normal distribution with zero mean and standard deviation σ_e. Thus, the noisy measurement position is $\tilde{\mathbf{l}}^i = \mathbf{l}^i + \mathbf{e}$. Fig. 6 illustrates the impact of position error with an increase in σ_e. Note that there is a noticeable improvement in $\mathscr{P}_{\text{D}}^{N}$ with M increasing from 50 to 100. When $\sigma_e \geq 3\,\text{m}$, $\mathscr{P}_{\text{D}}^{N-1}$ boosts sharply, and so is $\mathscr{E}_{\text{pos}}^{N-1}$ for both M. Moreover, for $M = 50$, $\mathscr{E}_{\text{pos}}^{N+1}$ increases gradually with a very low $\mathscr{P}_{\text{D}}^{N+1}$, while for $M = 100$, $\mathscr{P}_{\text{D}}^{N+1}$ becomes negligible confirming the underestimation of the number of PUs. It is also worth noting that $\mathscr{E}_{\text{pos}}^{N}$ outperforms $\mathscr{E}_{\text{pos}}^{\text{sgl}}$ due to the combination of score maps on multiple PUs.

VI. Conclusion

In this work, we proposed a non-collaborative multiple PU localization algorithm in a UAV assisted scenario. The algorithm requires only RSS and SoA measurements to build up the score map and perform PU number detection and localization by hierarchical clustering and WCL. The performance is evaluated by the probability of detecting the PUs and the RMSE of the localization error. Numerical results have shown that with a proper choice of the parameters, the methodology proposed can achieve a high probability of detecting the right number of PUs and low RMSE even in the presence of channel impairments and UAV position uncertainties.

References

[1] Y. Zeng, R. Zhang, and T. J. Lim, "Wireless communications with unmanned aerial vehicles: Opportunities and challenges," *IEEE Comm. Mag.*, vol. 54, no. 5, pp. 36–42, May 2016.

[2] Y. Zou and Q. Wan, "Emitter source localization using time-of-arrival measurements from single moving receiver," in *Proc. IEEE Int. Conf. on Acoustics, Speech and Signal Proc. (ICASSP)*, New Orleans, LA, USA, Jun. 2017, pp. 3444–3448.

[3] J. Tiemann, F. Eckermann, and C. Wietfeld, "ATLAS - An open-source TDOA-based Ultra-wideband localization system," in *Proc. IEEE Int. Conf. on Indoor Pos. and Indoor Nav. (IPIN)*, Alcala de Henares, Spain, Nov. 2016, pp. 1–6.

[4] K. Magowe and S. Kandeepan, "Cooperative blind localization of primary user in a cognitive radio environment," in *Proc. IEEE Int. Conf. on Signal Proc. and Comm. Sys. (ICSPCS)*, Gold Coast, Australia, Dec. 2014, pp. 1–8.

[5] K. Magowe, A. Giorgetti, S. Kandeepan, and X. Yu, "Accurate analysis of weighted centroid localization," *IEEE Trans. on Cognitive Comm. and Netw.*, vol. 5, no. 1, pp. 153–164, Mar. 2019.

[6] K. Magowe, A. Giorgetti, and S. Kandeepan, "Closed-form approximation of weighted centroid localization performance," *IEEE Sensors Letters*, vol. 3, no. 12, pp. 1–4, Dec. 2019.

[7] A. Giorgetti, K. Magowe, and S. Kandeepan, "Exact analysis of weighted centroid localization," in *Proc. IEEE European Signal Proc. Conf. (EUSIPCO)*, Budapest, Hungary, Aug. 2016, pp. 743–747.

[8] H. Lim, K. Lim, I. Joo, J. B. Kim, and S. U. Lee, "Experimental Performance of Signal Source Localization Based on Distributed DoA Measurements," in *Proc. IEEE Int. Technical Conf. on Circuits/Systems, Comp. and Comm. (ITC-CSCC)*, JeJu, Korea (South), Jun. 2019.

[9] R. K. Martin, "Wireless network discovery via RSS-based estimation of multi-transmitter RF footprint," in *Proc. IEEE Int. Work. on Comp. Advances in Multi-Sensor Adaptive Proc. (CAMSAP)*, Aruba, Dutch Antilles, Netherlands, Aug 2009, pp. 336–339.

[10] J. K. Nelson, M. R. Gupta, J. E. Almodovar, and W. H. Mortensen, "A quasi EM method for estimating multiple transmitter locations," *IEEE Signal Proc. Letters*, vol. 16, no. 5, pp. 354–357, Mar. 2009.

[11] P. Mankar, R. V. Rajakumar, and S. S. Pathak, "Likelihood criteria based co-channel primary transmitters localization algorithm for cognitive radio networks," in *Proc. IEEE Tencon - Spring*, Sydney, NSW, Australia, Apr. 2013, pp. 411–415.

[12] A. A. Redwan Newaz, S. Jeong, H. Lee, H. Ryu, and N. Y. Chong, "UAV-based multiple source localization and contour mapping of radiation fields," *Robotics and Auto. Sys.*, vol. 85, pp. 12–25, Nov. 2016.

[13] Z. Li, K. Magowe, A. Giorgetti, and S. Kandeepan, "Blind localization of primary users with sectorial antennas," in *Proc. IEEE Int. Conf. on Comm. Work. (ICC Work.)*, Kansas City, MO, USA, May 2018, pp. 1–6.

[14] Z. Li, S. Kandeepan, A. Giorgetti, A. Al-hourani, and K. Magowe, "Directional antenna channel modelling in urban area using ray tracing," *ITU Journal: ICT Discoveries*, vol. 2, no. 1, Nov. 2019.

[15] A. Al-Hourani, S. Kandeepan, and A. Jamalipour, "Modeling air-to-ground path loss for low altitude platforms in urban environments," in *Proc. IEEE Global Comm. Conf.*, Austin, TX, USA, Dec. 2014, pp. 2898–2904.

[16] N. H. Ranchagoda, S. Kandeepan, M. Ding, U. Thayasivam, and K. M. Gomez, "A building height-dependent gaussian mixture model to characterize air-to-ground wireless channels," in *Proc. IEEE Int. Conf. on Comm. Sys.*, Chengdu, China, Dec. 2018, pp. 173–179.

[17] A. Mariani, S. Kandeepan, A. Giorgetti, and M. Chiani, "Cooperative weighted centroid localization for cognitive radio networks," in *Proc. IEEE Int. Symp. on Comm. and Inf. Tech., (ISCIT)*, Gold Coast, Australia, Oct. 2012, pp. 459–464.